Precision Rotation Measurements with an Atom Interferometer Gyroscope

T. L. Gustavson, P. Bouyer,* and M. A. Kasevich

Department of Physics, Stanford University, Stanford, California 94035
(Received 10 September 1996)

We report the demonstration of a Sagnac-effect atom interferometer gyroscope which uses stimulated Raman transitions to coherently manipulate atomic wave packets. We have measured the Earth's rotation rate, and demonstrated a short-term sensitivity to rotations of 2×10^{-8} (rad/s)/$\sqrt{\text{Hz}}$. [S0031-9007(97)02734-8]

Matter-wave interferometry has the potential to be an extremely sensitive probe for inertial forces. For example, neutron interferometers have been used to measure the rotation of the Earth [1] and the acceleration due to gravity [2]. More recently, atom interference techniques have been used in demonstration experiments to measure rotations [3] and accelerations [4]. In this Letter, we present an atom-based Sagnac gyroscope that has a short-term sensitivity comparable to state-of-the-art optical gyroscopes [5,6], and is at least 2 orders of magnitude better than previous matter-based experiments [1,3,7].

In the Sagnac geometry [8], rotation induces a phase shift $\Delta\phi$ between two interfering propagation paths. For a Sagnac loop enclosing area **A**, a rotation $\mathbf{\Omega}$ produces a shift $\Delta\phi = \frac{4\pi}{\lambda v}\mathbf{\Omega} \cdot \mathbf{A}$, where λ is the particle wavelength and v its velocity [9–11]. Thus the inherent sensitivity of a matter-wave gyroscope exceeds that of a photon-based system by a factor of $mc^2/\hbar\omega \sim 10^{11}$ (m is the particle mass, ω the photon frequency). Although optical gyroscopes have higher particle fluxes and larger enclosed areas, atom-based systems should still out-perform optical systems by several orders of magnitude. Higher precision gyroscopes could find practical applications in navigation or in geophysical studies. They could also be used in tests of general relativity [6,12,13]. For example, one might realize a ground-based detection of the dragging of inertial frames [14].

We have developed an atomic state interferometer [15] which uses two-photon velocity selective Raman transitions [16,17] to manipulate atoms while keeping them in long-lived ground states. With the Raman method, two laser beams of frequency ω_1 and ω_2 are tuned to be nearly resonant with an allowed optical transition. Their frequency difference $\omega_1 - \omega_2$ is chosen to be resonant with a microwave transition between two atomic ground-state levels. Under appropriate conditions, the atomic population Rabi flops between the ground-state levels with a rate proportional to the product of the two single-photon Rabi frequencies and inversely proportional to the optical detuning. When the beams are aligned to counterpropagate, a momentum exchange of approximately twice the single-photon momentum accompanies these transitions. This leads to a strong Doppler sensitivity of the two-photon

transition frequency, and can be used to coherently divide (with a $\pi/2$ pulse) or deflect (with a π pulse) atomic wave packets. (On the other hand, when the beams are aligned to copropagate, these transitions have a negligible effect on the atomic momentum, and the transition frequency is Doppler insensitive.) A Mach-Zehnder-type interferometer is formed using a $\pi/2$-π-$\pi/2$ pulse sequence to coherently divide, deflect, and finally recombine atomic wave packets. The resulting interference can be directly observed by measuring the atomic ground-state populations [18].

Our experimental setup is shown in Fig. 1. An effusive beam of cesium atoms is collimated by two 1 mm diameter apertures and transversely cooled in a 2D optical molasses [19,20]. The resulting beam has a flux of $\sim 6 \times 10^8$ atoms/s with a most probable longitudinal velocity of 290 m/s and a transverse velocity spread of 10 cm/s (0.3 mrad collimation). The base pressure of the vacuum system is $\sim 5 \times 10^{-9}$ Torr.

We drive stimulated Raman transitions between the Cs $6S_{1/2}, F = 3, m_F = 0$ and $6S_{1/2}, F = 4, m_F = 0$ magnetic field insensitive ground-state hyperfine levels. State preparation was accomplished by first optically pumping the atoms into the $F = 4, m_F = 0$ level with $\sim 95\%$ efficiency
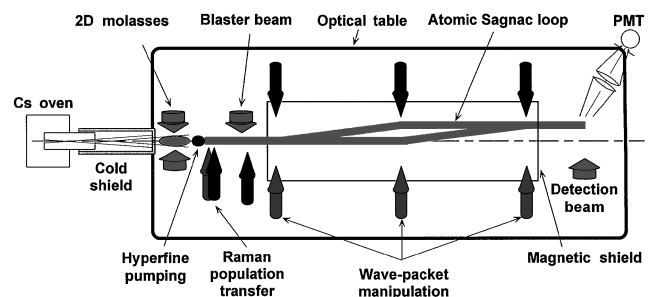
FIG. 1. Experimental apparatus. A cesium atomic beam is collimated and transversely cooled in a two-dimensional molasses. The atoms are then optically pumped into a magnetic field insensitive hyperfine state before entering the 2 m long magnetically shielded interrogation region of the vacuum chamber. Two-photon stimulated Raman transitions are used to drive the $\pi/2$-π-$\pi/2$ interferometer pulse sequence. Atoms making the ground state $F = 3 \rightarrow F = 4$ transition are detected by resonance fluorescence.

[21,22]. We then transferred the atoms from the $F = 4, m_F = 0$ to the $F = 3, m_F = 0$ level with a π Raman pulse (Doppler insensitive). Residual atoms remaining in the $F = 4$ states were blown away by a resonant blaster beam. We use this three-step scheme to enable efficient detection on a cycling transition. It also allows for clean state preparation and improves longitudinal velocity collimation.

Following state preparation, atoms enter a ~ 2 m long, magnetically shielded, interrogation region. In this region three pairs of counterpropagating beams are used to drive the Raman transitions. The beams are oriented perpendicular to the atomic beam in a horizontal plane, with a 0.96 m separation between each pair. The atoms begin in the $|F = 3, m_F = 0; p_0\rangle$ state upon entering the interrogation region (p_0 is the initial momentum). The first $\pi/2$ pulse puts the atoms in a superposition of $|F = 3, m_F = 0; p_0\rangle$ and $|F = 4, m_F = 0; p_0 + 2\hbar k\rangle$ states. (The two-photon recoil momentum $2\hbar k$ corresponds to a 7 mm/s transverse velocity.) The two wave packets then separate by on average 23 μm during ~ 1 m of free flight. Next, they pass through the π Raman beams, which exchange the two ground states and momenta. The redirected trajectories meet again after ~ 1 m, where the last $\pi/2$ pulse overlaps the two wave packets. The average total area enclosed by the interferometer is 22 mm^2. Atoms which made the transition from the $F = 3$ to the $F = 4$ state are detected by a resonant probe laser beam tuned to the $6S_{1/2}, F = 4 \rightarrow 6P_{3/2}, F = 5$ cycling transition. The resulting fluorescence was imaged onto a photomultiplier tube. An average of 1.2 photons per atom was detected.

The implementation of our Raman laser system has been described in detail in a prior publication [23]. Briefly, 852 nm light from a distributed Bragg reflector diode laser passes through a 4.6 GHz acousto-optic modulator and is retroreflected. The $+1$ and -1 diffracted orders are amplified by optical injection locking two 150 mW diode lasers. The injected lasers have a stable frequency difference of 9.2 GHz, the cesium clock frequency corresponding to transitions between the $F = 3$ and $F = 4$ ground states. After passing through optical isolators the output beams are spatially filtered and expanded to a 1.1 cm $1/e^2$ diameter.

As the Raman lasers run continuously, the atoms see a pulse area determined by their time of flight through the laser beams. Vertical slits of width 5.5 mm were placed in front of the Raman beam windows to set the pulse length. A uniform 200 mG bias field is applied along the axis of the Raman beams to maintain well-defined internal atomic states in the interrogation region. The Raman lasers were detuned from the 852 nm D_2 line by $\Delta = -3.0$ GHz to avoid spontaneous emission. The intensity of the laser beam coupling the $6S_{1/2}, F = 4$ and $6P_{3/2}$ levels was twice that of the beam coupling the $6S_{1/2}, F = 3$ and $6P_{3/2}$ levels. This intensity ratio balanced the Raman laser-induced ac Stark shifts of the ground-state levels. When unbalanced, the resonance frequencies in the $\pi/2$ and π regions were offset by an amount comparable with the transition linewidth.

We first observed interference fringes by varying the optical phase of the final $\pi/2$ pulse (Fig. 2). This was achieved either by tilting a phase plate located in the beam path of one of the two Raman laser beams just before the final $\pi/2$ region or by scanning the horizontal alignment of one of these beams. The maximum contrast is about 20% when the Raman beam propagation axes are parallel [24]. The fringe peak-to-peak amplitude is $\simeq 10^7$ atoms/s. The noise level is currently limited by scattered light from the detection beam which creates a background ~ 10 times the fringe signal.

We rotated the propagation axes of the three Raman beam pairs simultaneously in the horizontal plane to observe the Sagnac phase shift. This was done by applying a sinusoidally varying force to the (floating) optical table on which the Raman beam optics were mounted. A piezoelectric transducer (PZT) anchored to the floor through a separate vibrationally isolated platform was used for this purpose. We independently measured the rotation rate of the table with a calibrated seismometer (Kinemetrics SS1). Figure 3 shows the variation of the interfering signal with the rotation rate inferred from the seismometer. The integration time was 800 ms per point. The loss of contrast for large rotation rates is due to the averaging of the Sagnac phase shift over the longitudinal velocity distribution. A signal-to-noise ratio of 400 : 1 can be extracted from a fit to the central fringe. The corresponding short-term sensitivity is 2×10^{-8} (rad/s)/$\sqrt{\text{Hz}}$.

The center of the contrast envelope does not correspond with the zero rotation rate measured by the seismometer. Since the seismometer is not sensitive to dc rotations, but the gyroscope is, the signal is offset by the Earth's rotation rate. In order to quantify this offset we fit a model
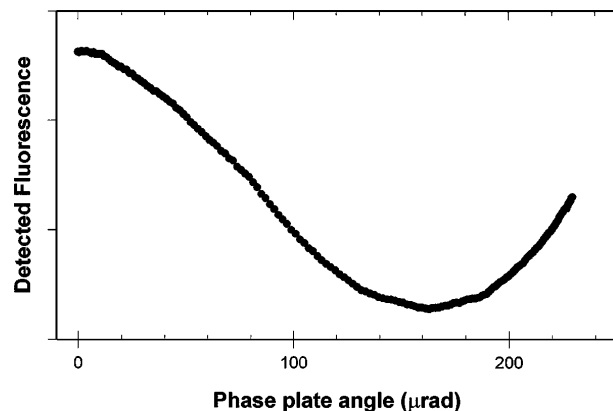
FIG. 2. Atoms in the $F = 4$ state detected at the exit of the interrogation region as a function of the optical phase of the final $\pi/2$ pulse. The phase is scanned by rotating a 0.5 in. plate in the optical path of one of the Raman beams.
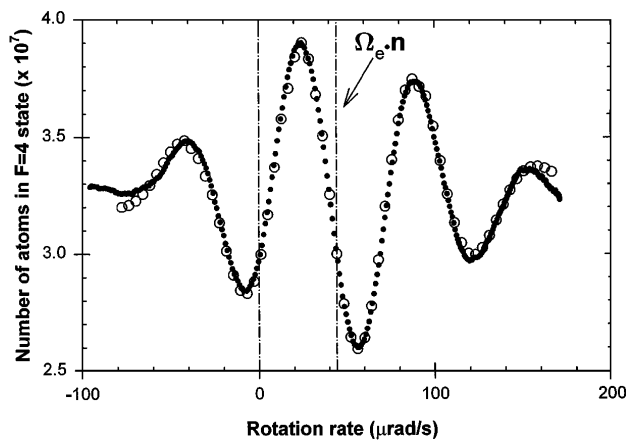
FIG. 3. Measurement of an atom interference pattern versus rotation rate. Black dots: experimental data. Open circles: calculated signal. The shift of the contrast envelope provides a measurement of the Earth's rotation rate.

to the signal with the offset as an adjustable parameter, as show in Fig. 3. To calculate the modeled signal we treat the atomic trajectories and the Raman transitions semiclassically. In this model we chose the viewpoint that the Sagnac phase shift arises from the atom's interaction with the rotating laser beams [25]. The model includes averages over the measured longitudinal and transverse velocity distributions, but does not include averages over the transverse spatial profiles of the Raman or atomic beams. It also accounts for an arbitrary (experimentally uncontroled) initial optical phase offset, which determines the fringe location within the contrast envelope. We omit higher order rotation terms and corrections for the change in the rotation rate during the atom's time of flight through the interferometer, both of which are negligible for our operating conditions. From the fit we extract a Sagnac phase shift of 4.2 rad, which corresponds to a rotation offset of 45 ± 3 μrad/s. The uncertainty is due to the calibration of the seismometer. At our latitude the projection of the Earth's rotation rate $\mathbf{\Omega}_e \cdot \mathbf{n}$ (where $\mathbf{n} \equiv \mathbf{A}/|\mathbf{A}|$) is 44.2 μrad/s, which is consistent with our measured value. The discrepancy between the calculated and observed wave forms at large rotation rates is not fully understood.

We investigated the gyroscope's sensitivity for different integration times. For these measurements we applied a sinusoidal varying rotation rate to the table. The maximum rotation rate was typically set between 50 nrad/s and 1 μrad/s. This resulted in a phase modulation of the signal $\delta\phi \ll \pi$ rad. We set the operating point on the side of a fringe to increase our sensitivity to small rotations. We servoed the angle of the final Raman beam with a PZT to keep the signal locked to this operating point. This compensated for slow phase drifts, primarily due to air currents, and allowed for integration times as long 10^4 s. In this scheme the rotation-induced phase modulation appears on the lock feedback signal. It was analyzed in

the frequency domain using a low frequency spectrum analyzer (HP3562A). We show the results of a typical measurement in Fig. 4.

Alignment of the Raman beams is critical for obtaining good fringe contrast [24]. The beams need to be aligned to within 10^{-4} rad to observe interference. The horizontal alignment can be set by exploiting the Doppler sensitivity of the Raman transitions. The Raman resonances in the π and $\pi/2$ regions occur at the same rf frequency when the Raman beams are parallel. In the vertical direction we had no Doppler shift diagnostic. Instead, we aligned all six beams normal to a vertical reference mirror using optical interferometric methods. A tilt sensor attached to the reference mirror mount was used to define the vertical plane to within 10^{-4} rad. This alignment technique suppresses gravitational phase shifts and centripetal phase shifts arising from the Earth's rotation.

Vibration isolation of the optical table (Newport RS-4000 floating on I-2000 legs) is also essential. Rotational and translational noise produces random phase shifts on the interference signal. The vacuum chamber was mounted on a freestanding platform just above the optical table to prevent vacuum pump vibrations from coupling to the Raman laser beams. Highly stable mirror mounts were used for the Raman optics and in other key beam paths to avoid vibration-induced optical phase shifts and beam pointing variations. Optical phase shifts due to convection have been reduced by enclosing the Raman beams in 1 in. diameter tubes.

It is useful to compare our Raman transition method with other coherent atom manipulation techniques. In comparison with mechanical nanofabricated gratings [26], optical gratings can be easily vibrationally isolated from the vacuum chamber. Scattering from standing waves [27,28] can be efficient and capable of large momentum transfer. However, these beam splitters typically require a highly collimated atomic beam. In contrast, the stimulated Raman transition linewidth can be adjusted to address large
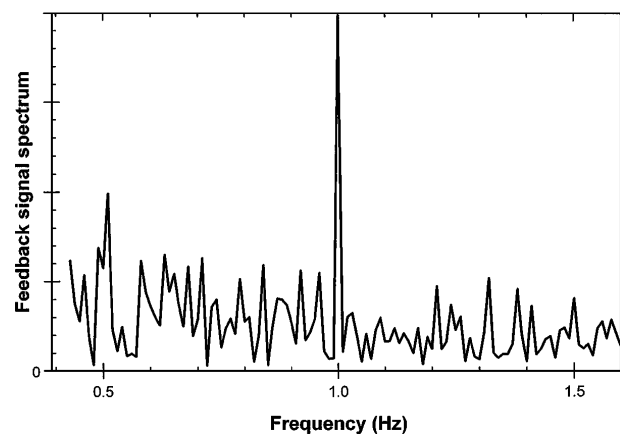
FIG. 4. Power spectrum of the servo error signal corresponding to a 1 Hz, 60 nrad/s rms rotational excitation of the optical table after 10^3 s.

transverse velocity spreads, relaxing collimation requirements and increasing interferometer count rates.

We can still improve the short-term sensitivity. We are installing higher flux cesium ovens which will increase our count rate by a factor of 100. Because sensitivity scales with the square of the length of the interferometer, a longer apparatus could yield significant improvement. Larger interferometer areas might also be achieved using multiple Raman pulse sequences [29] or a slower atomic beam.

We are also installing a second, counterpropagating, atomic beam. When each atomic beam is aligned to interact with the same set of Raman beams, the area vectors for the resulting Sagnac loops have opposite directions, and the corresponding phase shifts $\Delta\phi$ have opposite signs. Taking the difference between the two phase shifts, common mode rejects many systematic errors which do not reverse sign with the direction of the atomic beam. These include phase shifts arising from uniform accelerations. It also reduces sensitivity to low frequency optical phase fluctuations, and should significantly improve long-term stability.

In conclusion, we have demonstrated a gyroscope based on velocity sensitive Raman transitions which has a 2×10^{-8} (rad/s)/$\sqrt{\text{Hz}}$ short-term sensitivity. We believe this to be 2 orders of magnitude better than any other existing atom interferometer and comparable to the best active ring laser gyroscopes [5]. By making straightforward improvements, we hope to increase performance by twentyfold to 1×10^{-9} (rad/s)/$\sqrt{\text{Hz}}$. Care has been taken to make the apparatus stable to allow the possibility of integrating for long periods of time ($\sim 10^4$ s). Long-term stability is crucial for many gyroscope applications, and we plan to study this in future work.

*Present address: Institut d'Optique, BP 147, 91403 Orsay Cedex, France.

[1] R. Colella, A. Overhauser, and S. Werner, Phys. Rev. Lett. **34**, 1472 (1975).

[2] S. A. Werner, J. L. Staudenmann, and R. Colella, Phys. Rev. Lett. **42**, 1103 (1979).

[3] F. Riehle *et al.*, Phys. Rev. Lett. **67**, 177 (1991).

[4] M. Kasevich and S. Chu, Appl. Phys. B **54**, 321 (1992).

[5] G. Stedman *et al.*, Phys. Rev. A **51**, 4944 (1995).

[6] W. Chow *et al.*, Rev. Mod. Phys. **57**, 61 (1985).

[7] J. Schmiedmayer *et al.*, in *Atom Interferometry*, edited by P. Berman (Academic Press, New York, 1997), pp. 2–83.

[8] M. Sagnac, C. R. Acad. Sci. **157**, 708 (1913).

[9] Ch. J. Bordé, in *Laser Spectroscopy X*, edited by M. Ducloy, E. Giacobino, and G. Camy (World Scientific, Singapore, 1992), pp. 239–245.

[10] P. Storey and C. Cohen-Tannoudji, J. Phys. II (France) **4**, 1999 (1994).

[11] This expression is for particles interfering after traversing half of the loop. In the original Sagnac geometry, the particles interfere after counterpropagating around the full loop, yielding an additional factor of 2.

[12] J. F. Clauser, Physica (Amsterdam) **151B**, 262 (1988).

[13] Ch. J. Bordé, A. Karasiewicz, and Ph. Tourrenc, Int. J. Mod. Phys. D **3**, 157 (1994).

[14] M. Cerdonio, G. A. Probi, and S. Vitale, Gen. Relativ. Gravit. **20**, 83 (1988).

[15] Ch. J. Bordé, Phys. Lett. A **140**, 10 (1989).

[16] M. Kasevich *et al.*, Phys. Rev. Lett. **66**, 2297 (1991).

[17] K. Moler, D. S. Weiss, M. Kasevich, and S. Chu, Phys. Rev. A **45**, 342 (1992).

[18] M. Kasevich and S. Chu, Phys. Rev. Lett. **67**, 181 (1991).

[19] A. Aspect *et al.*, Chem. Phys. **145**, 307 (1990).

[20] P. D. Lett *et al.*, J. Opt. Soc. Am. B **6**, 2084 (1989).

[21] P. Tremblay and C. Jacques, Phys. Rev. A **41**, 4989 (1990).

[22] B. Masterson, C. Tanner, H. Patrick, and C. Wieman, Phys. Rev. A **47**, 2139 (1993).

[23] P. Bouyer, T. Gustavson, K. Haritos, and M. Kasevich, Opt. Lett. **21**, 1502 (1996).

[24] Specifically, $(k_1 - 2k_2 + k_3) \cdot w \ll \pi$, where w is the transverse spatial extent of the atomic beam, and k_i are the effective propagation vectors (see Ref. [4]) for the Raman transitions.

[25] There are other equivalent viewpoints. See, for example, Refs. [9] and [10].

[26] D. W. Keith, C. R. Ekstrom, Q. A. Turchette, and D. E. Pritchard, Phys. Rev. Lett. **66**, 2693 (1991).

[27] D. M. Giltner, R. W. McGowan, and S. A. Lee, Phys. Rev. Lett. **75**, 2638 (1995).

[28] E. M. Rasel *et al.*, Phys. Rev. Lett. **75**, 2633 (1995).

[29] B. Young, M. Kasevich, and S. Chu, in *Atom Interferometry*, edited by P. Berman (Academic Press, New York, 1997), pp. 363–406.